Third Quarterly Progress Report

March 27 through June 27, 1986

NIH Contract N01-NS-5-2396

Speech Processors for Auditory Prostheses

Prepared by

Charles C. Finley, Blake S. Wilson and Dewey T. Lawson

Neuroscience Program Office
Research Triangle Institute
Research Triangle Park, NC 27709

CONTENTS

I. Introduction

The purpose of this project is to design and evaluate speech processors for auditory prostheses. Ideally, the processors will extract (or preserve) from speech those parameters that are essential for intelligibility and then appropriately encode these parameters for electrical stimulation of the auditory nerve. Work in the present quarter included the following:

1. Evaluation of multiple processors in single tests of consonant and vowel recognition, where the presentations of both tokens and processors were randomized;

2. Evaluation of idealized versions of the processing strategy used in Melbourne/Nucleus device;

3. Evaluation of selected processing strategies with the vowel- and consonant-confusion tests developed by the implant team at the University of Iowa;

4. Development and testing of new computer programs to support and extend studies of processor performance;

5. Initial development of a portable, real-time processor for implementing various multichannel coding strategies, including the "interleaved-pulses" strategies described in our last quarterly progress report;

6. Preliminary analysis of field pattern data obtained by recording induced artifact potentials at non-stimulated electrodes in a patient fitted with a percutaneous cable; and

7. Presentation of project results in invited lectures at the Kresge Hearing Research Institute in Ann Arbor and at the Conference on Speech Recognition with Cochlear Implants in New York.

In this report we will describe our work on the development of realtime, portable speech processors and will present initial field pattern results with the percutaneous cable measurements. Detailed description of the studies of speech recognition is deferred for now, but will be presented in a future report.

II. Initial Development of Real-Time, Portable Processors

The primary objective of our real-time speech processor development is to provide connected-speech presentations using the best processing strategies as identified by experiments with the block-diagram compiler (see QPR 2, NIH project NO1-NS-5-2396). Of particular interest is real-time implementation of the six channel, interleaved-pulses processor with round-robin updates of all six channels. This processor is not only the best identified processor to date for patient MH but is also one of the more computationally demanding designs. Therefore, a flexible hardware implementation of this processing strategy will provide the basis for real-time implementation and testing of most of the other processing strategies previously implemented with the block-diagram compiler.

This hardware development is being pursued in three phases. Phase I is the development of a real-time, bench-level processor that will at minimum fully implement all of the features of processors simulated with the block-diagram compiler. This bench-level processor is intended as both a flexible research tool and as a prototype design for later wearable processors. The phase I bench-level processor interfaces to the patient through our existing laboratory stimulation equipment (Tech. Proposal B, RTI, NIH RFP No. NIH-NINCDS-85-09). In this case, the microprocessor generates a parallel 16-bit data stream which mimics the output of the block-diagram compiler system. Phase II is a wearable, hardware CHMOS implementation of the flexible processor system designed in Phase I. This wearable processor will allow short-term evaluations of promising processor strategies by patients in environments outside of the laboratory. The physical package of the Phase II processor will be larger than final, permanent wearable processors due to the extra flexibility that is being incorporated into this system. The Phase II wearable processor interfaces to the patient via multiplying DAC's and voltage/current drivers which are memory-mapped on the microcontroller address bus. Phase III is the final development of the wearable processor that the patient will use permanently. This design will be a highly optimized implementation of the best strategy identified using the previously described processors. Since many of the engineering decisions are dictated both by the information processing requirements of the processor design (processor cycle time, number of channels, number of bits) and by the constraints of achieving a final wearable device (chip packaging,

power requirements), all three development phases are being planned simultaneously. Actual construction of ~~the plans for~~ each phase of development will occur sequentially, beginning with the Phase I bench-level, real-time system. Experience gained from the actual use of each hardware design, coupled with reviews of the speech encoding performance of each design, will guide final plans for subsequent processor development, ultimately progressing to a final wearable processor.

As described previously (QPR 2, NIH project NO1-NS-5-2396), the interleaved-pulses processors provide the best performance to date in confusion matrix tests. In these processors input speech signals are first high-pass filtered to flatten the speech spectrum and diminish the otherwise overwhelming influence of the first formant (F1). The output of the high-pass filter is then fed to a bank of bandpass filters whose center frequencies span the combined range of F1 and F2, along a logarithmic scale. The RMS energy in each band is sensed by a full-wave rectifier and a low-pass filter connected in series to each bandpass filter output. Next, a "post-processor" is programmed to scan the RMS outputs each time a pulse is to be delivered to the electrode array. The output of a filter bank channel is delivered to its assigned electrode(s) only if (a) it is one of the N channels with the greatest RMS energy for the present time frame and (b) the RMS energy is above a preset "noise threshold" (where N is the total number of channels to be updated at any one time and may vary from 1 to 8). Finally, the amplitudes of the pulse(s) delivered to the selected channel(s) in the electrode array are derived with a logarithmic mapping law for each channel.

Figure 1 shows a block diagram of this basic architecture for implementation in Phase I and Phase II real-time processor development. The processor is divided into four subsections including a signal conditioner, a filter bank, a post-processor and channel drivers. Each subsection is discussed below.

The signal conditioner provides all filtering and gain control necessary to map microphone signals into the filter bank. The single pole high-pass filter reduces the first formant contribution. The variable gain stage is the forward path controlling element in an AGC loop and is controlled by the post-processor. This gain stage is incorporated in the filter bank as described below.

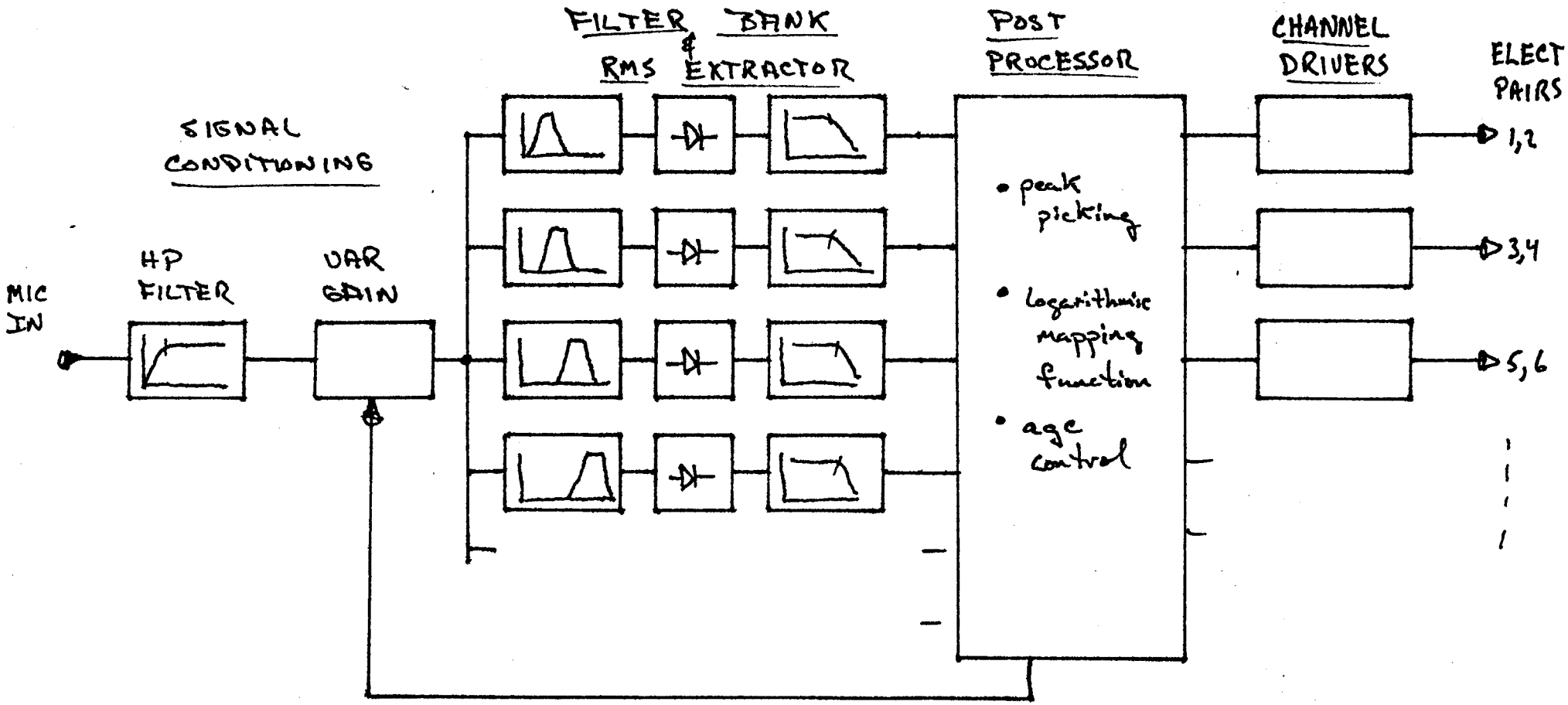
FILTER BANK & RMS EXTRACTOR
POST PROCESSOR
CHANNEL DRIVERS
ELECT PAIRS
SIGNAL CONDITIONING
MIC IN
HP FILTER
VAR GAIN
• peak picking
• logarithmic mapping function
• age control
1,2
3,4
5,6

FIGURE 1.

Filter bank extractions with RMS outputs are achieved with a single uPD7763D NEC speech analysis chip for speech recognition systems (Fig. 2a). The uPD7763D incorporates a programmable pre-amp with optional equalizer, a 16-channel switched-capacitor band-pass filter bank (Fig. 2b), a multiplexed rectifier with switch-capacitor low-pass filters and S/H outputs (Fig. 2c), and an 8-bit A/D converter in a single LSI MOS 28-pin package. The uPD7763D has a general purpose microprocessor interface which provides access to a FIFO buffer containing digitized RMS outputs of band energies. Pre-amp gain (-13.5 dB to +33.0 dB), equalizer ON/OFF, analyzed frame period (1-32 msec) and low-pass filter cut-off frequency (12.5 Hz - 400 Hz) are controlled via the microprocessor interface. Analysis proceeds on a frame-by-frame basis with RMS levels for each bandpass during the previous frame being available in a FIFO buffer. A frame period signal is available as an external interrupt signal to the post-processor, which may then read the memory-mapped FIFO buffer. The uPD7763D typically consumes 175 mWatts of power (350 mWatts maximum).

The post-processor is an Intel 8031 8-bit microcontroller. This device features two 16-bit programmable timers with interrupt capability along with two external interrupt lines. The 8031 has 128 bytes of onboard RAM and can address 64k bytes of external program memory and 64k bytes of external data memory. Thirty-two programmable I/O lines and an asychronous serial port are available. A hardware multiplication and Boolean processing capability are also featured. This processor is available in CHMOS technology as the 80C31. The 80C31 additionally features two software selectable power down/idle modes for minimization of power consumption. In the powerdown mode the processor clock is turned off, where as in the idle mode the interrupt, asynchronous serial input and onboard timer operations continue to function. At 12 MHz clock operation (1 usec instruction period, typ), the 80C31 consumes 80 mW of power at full operation and 22.5 mW of power when idled. Memory for the Phase II and Phase III designs shall be either EPROM or EEPROM.

The Phase I and Phase II processor configurations use SIBEC development boards from Binary Technology, Meriden, NH. These single-board computers feature a fully supported 8031 or 80C31 microcontroller with conditioned I/O port and address/data busses available at connectors. The SIBEC board also supports a simple software monitor that facilitates downloading, execution and debugging of microcode for the 8031 microcontroller. Communication with

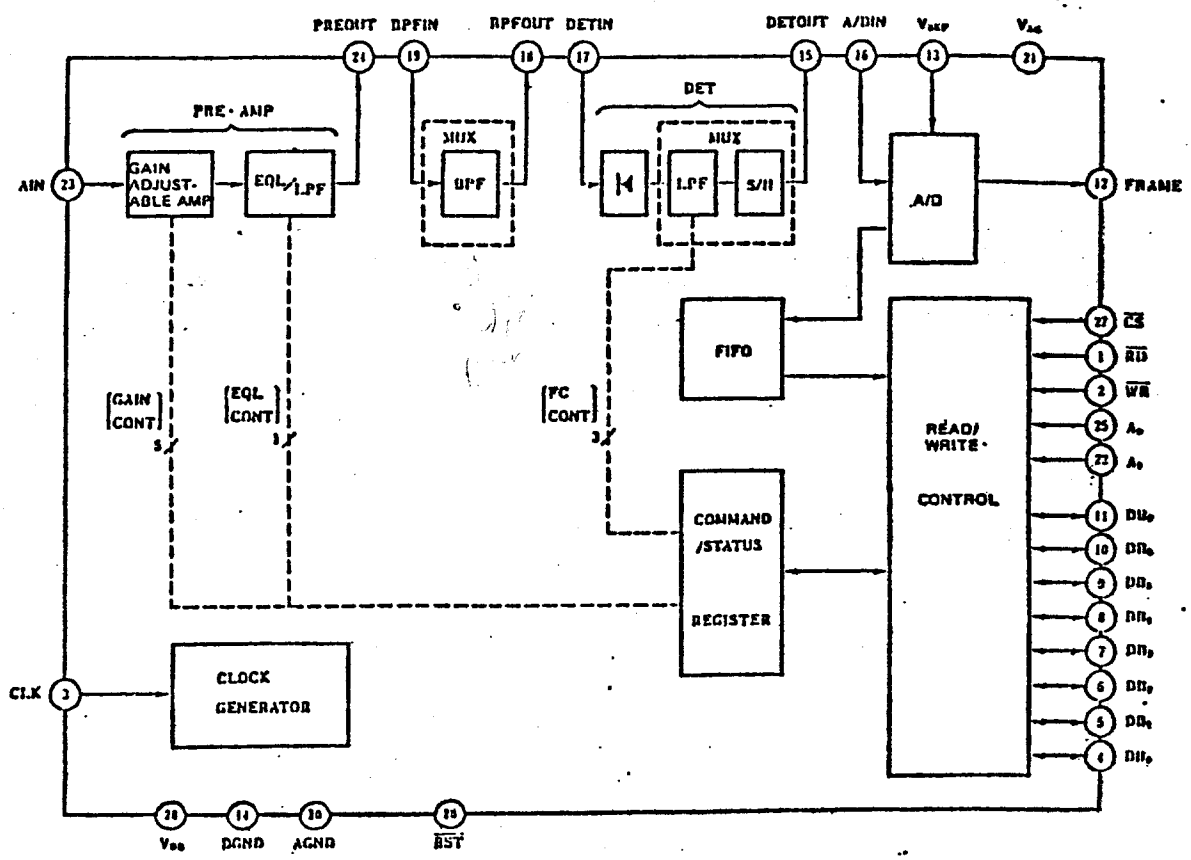

(a) Block diagram of uPD7763D NEC speech analysis chip.

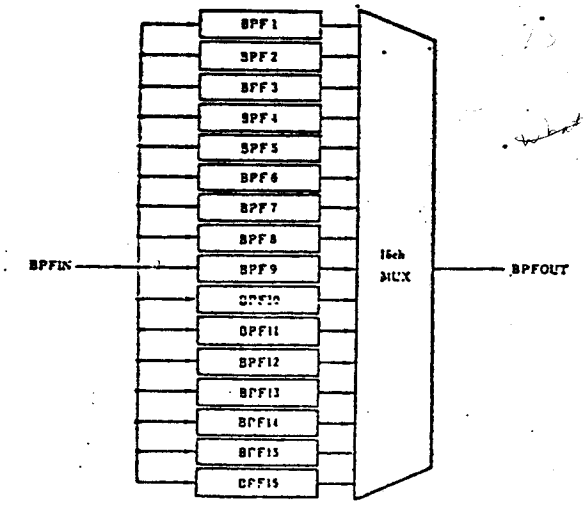

(b) Switched-capacitor filter bank with multiplexed output.

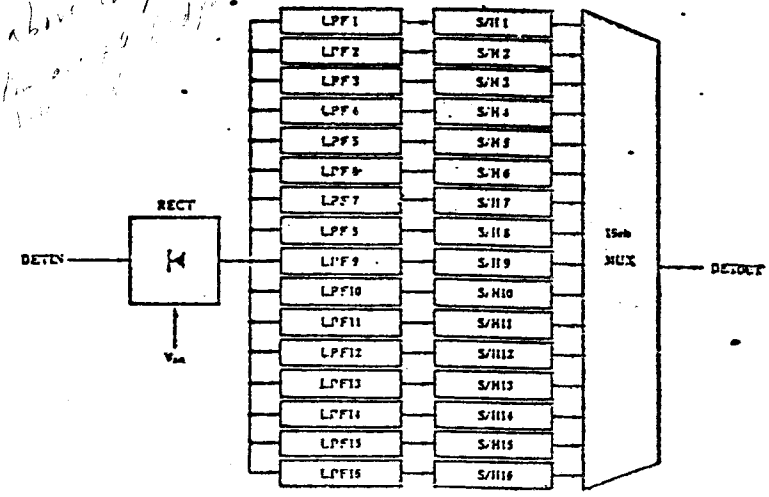

(c) Multiplexed RMS extractor featuring rectifier, low-pass filters and multiplexed S/H buffered outputs.

Figure 2.

the monitor is via the serial interface using an IBM-PC. Microcode is developed on the PC with a cross-assembler (Avocet Systems, Inc., Dover, Delaware).

Post-processor functions for the six-channel, interleaved-pulse processors include: (1) reading the filter bank FIFO for 16-bands of RMS levels; (2) condensing these sixteen bands down to the required six bands for the six-channel processor; (3) determining the temporal and amplitude stimulus features for each channel from previously defined lookup tables; and, (4) servicing the AGC control loop. Filter bank FIFO reading and the derivation of the RMS levels for each of the six channels is handled with one external interrupt task, synchronized to the completion of the filter bank analysis frame period. Round-robin updates for each channel are handled with a separate 10 kHz timer-driven interrupt subroutine which performs the necessary table lookups and passes the values to output driver stages. Table lookups are based on logarithmic loudness mapping functions relating the RMS bandpass signal level to output stimulus magnitude. To obtain the actual mapped output pulse train, two sets of tables are used. One table contains a normalized round-robin pulse (high-pass filtered) sequence for six channels of stimulation lasting for one filter bank analysis period. The other table contains the logarithmic mapping function for each channel. Multiplication of the normalized pulse sequences by the amplitude factor from the loudness mapping function is performed by the driver stages. One round-robin output sequence (10 kHz update rate) across six stimulus channels is made for each analysis frame period (2 msec) of the NEC uPD7763D chip.

Driver stage configuration differs for each phase of development of the real-time processors. The Phase I system, to be used as an extension of the block-diagram compiler in the laboratory, interfaces to our existing patient stimulation equipment via a digital link. The wearable Phase II system, seeking the same processor flexibility as Phase I, uses two cascaded CMOS multiplying DAC's with latched buffers. Four quadrant multiplication is used. DAC outputs are then directed to either a current/voltage driver stage for percutaneous cable patients or to the RF drivers for patients with the transcutaneous interface. The driver configuration for the final, wearable Phase III processor is undefined until further experience is gained with the Phase I and II systems.

The decision to structure the Phase I and Phase II processors as described provides maximal flexibility and speed in post-processor execution. A further addition under consideration includes of a second 80C31 microcontroller to the system for real-time extraction of F0 and voice/unvoiced boundaries using the Average-Magnitude-Difference-Function (AMDF) algorithm as described in QPR 6, NIH project N01-NS-2356. This would allow implementation of interleaved-pulses processors that have explicit representation of voicing information. Block-diagram compiler test results for processors with explicit voicing representation are described in QPR 2, NIH project N01-NS-5-2396. We are also investigating the feasibility of directly sampling the multiplexed-bandpass output of the NEC filter chip. This would allow the same hardware to simulate both the present UCSF/Storz analog processor and the interleaved-pulses strategies for more direct comparison of the two approaches.

Presently, the Phase I bench-level processor is nearing completion. The NEC filter bank has been interfaced to the 8031 microcontroller and debugged. The interface to the laboratory driver stages is presently being tested. We are now writing the software for implementing a six-channel, interleaved-pulses processor for real-time testing with patient MH in the laboratory. After an initial evaluation of this processor, Phase II construction of a CMOS version of the same processor will begin. If all goes well we hope to have a very flexible, programmable, take-home processor for patient MH within a month.

III. Analysis of Intracochlear Field Patterns as Measured via a Percutaneous Cable

We assume that the development of improved auditory prostheses is largely limited by our inability to exert control over the firing patterns of auditory nerve fibers. Toward understanding the complex relationships that govern and limit our ability to achieve desired firing patterns, we wish to know the potential distributions that exist within the stimulated cochlea, preferably the human cochlea. Two approaches are being pursued to provide such knowledge.

Firstly, a simple finite difference model of the field patterns around the UCSF/Storz electrode array has been developed. This model provides estimates of stimulation fields that are seemingly very limited in scope. In particular, a two-dimensional geometry is assumed as an approximation for a complex three-dimensional structure. Also, tissue characteristics are ignored by assuming a homogenous medium. Nevertheless, this model has served well as a heuristic tool by providing insight into the relative sensitivity to and significance of various features of the system. Figures 3 through 6 review this model and show data predicted by the model for a very simple stimulus. This work has been presented previously in more detail (QPR 5, NIH project N01-NS-2356). It is reviewed here to facilitate interpretation of the measured field patterns discussed below.

Secondly, we have attempted to directly measure intracochlear potentials in a patient (SG) who had a direct percutaneous cable connection to her intracochlear electrodes. The procedure consists of applying a continuous sinusoidal stimulus to one monopolar electrode or to a bipolar pair. Then we record the artifact potential appearing on the remaining non-stimulated electrodes in the array. In this manner, we seek to spatially sample the electrical field generated by the stimulated electrodes. Figures 7 through 11 describe the recording procedure, analysis method and initial results.

The results presented here represent an initial effort to analyze intracochlear potential data collected from a patient with a percutaneous cable. The model results are included as a comparision of the two methods and because the model serves a useful function in interpreting the recorded potentials.

Model Predictions

Figure 3 shows the position of each of the sixteen electrodes of the UCSF/Storz electrode array when viewed from above the plane of the electrode array spiral. Electrode positions are determined both by the electrode placement in the silastic carrier and by the spiral configuration of the array itself, the latter of which is fixed by the assembly's mechanical memory. Each electrode is indicated by closed circles, and the center line of the silastic carrier is shown by the spiral curve. Perpendicular to the spiral are short lines indicating the positions of radially-directed dendrites, spaced at one millimeter intervals along the spiral.

Figure 4 indicates how potential field patterns are calculated using the finite-difference method for stimulation of the two most apical electrodes in a bipolar manner. Electrode [1] is polarized with a positive voltage and electrode [2] is polarized with an equal, but negative, voltage. The tissue medium for calculations in the plane of the spiral is assumed to be homogeneous and therefore the results do not reflect possible effects of impedance differences at tissue boundaries. Computations are conducted with the outer boundary of the spiral plane held to zero. The right panel shows isopotential contours in the subsection of the plane. Also shown are the electrode locations and the spiral path of the electrode array. The locations of radial dendrites are labeled A-T, with an arrowhead pointing to the modiolar end of each dendrite. The left side of the figure indicates the potential levels along the locus of each dendrite, A-T. The ordinate of each small panel is voltage, ranging between the peak voltages applied to electrodes [1] and [2]. The abcissae indicate positions along the dendrites.

Figure 5 provides a high resolution picture of voltage profiles produed along the dendrites. In Figure 5 a continuum of dendrite positions is presented from the most-basal to the most-apical positions of the electrode array. The three panels show the extracellular stimulus voltage at the most-medial, the mid, and the most-lateral positions of the dendrites. The most-medial and the most-lateral positons also correspond to the relative positions of the medial and lateral electrodes in the spiral array. The abcissae indicate positions along the basilar membrane from basal to apical. The midpoint positions of each of the bipolar electrode pairs are indicated by the vertical lines, with the relative position of each electrode

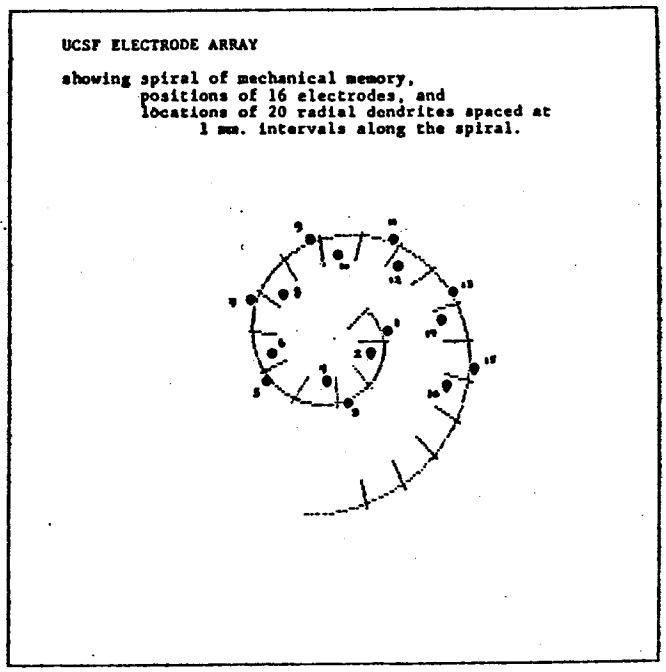

Figure 3.

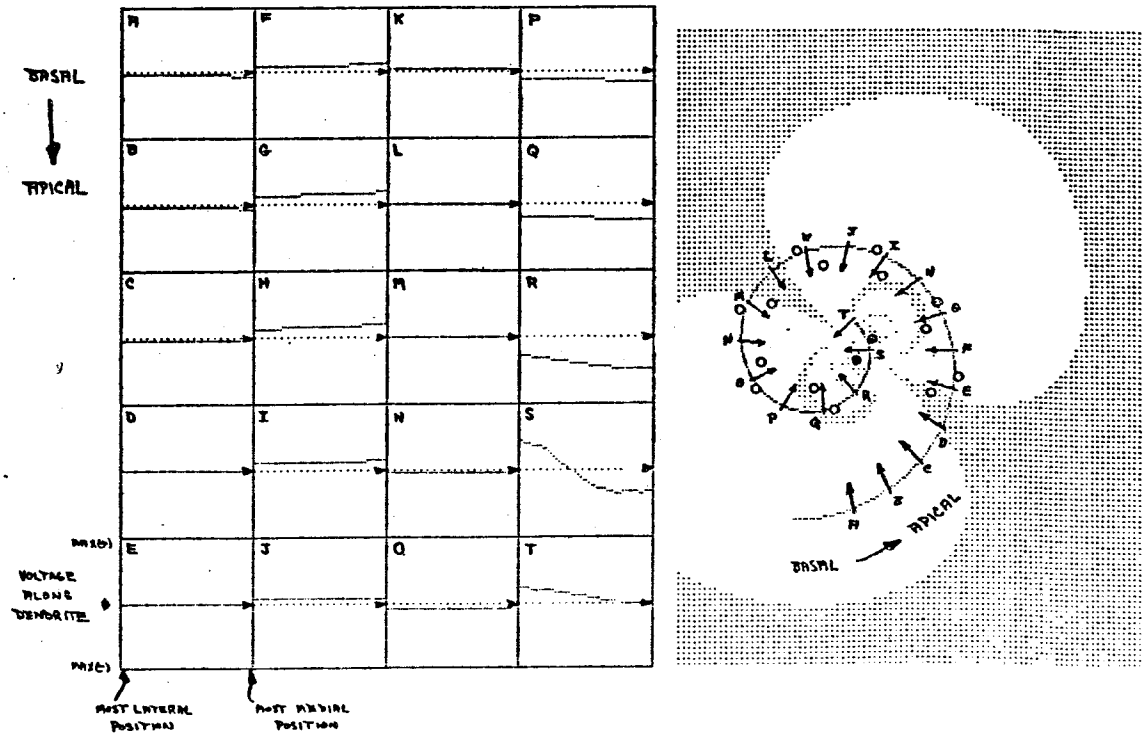

Figure 4.

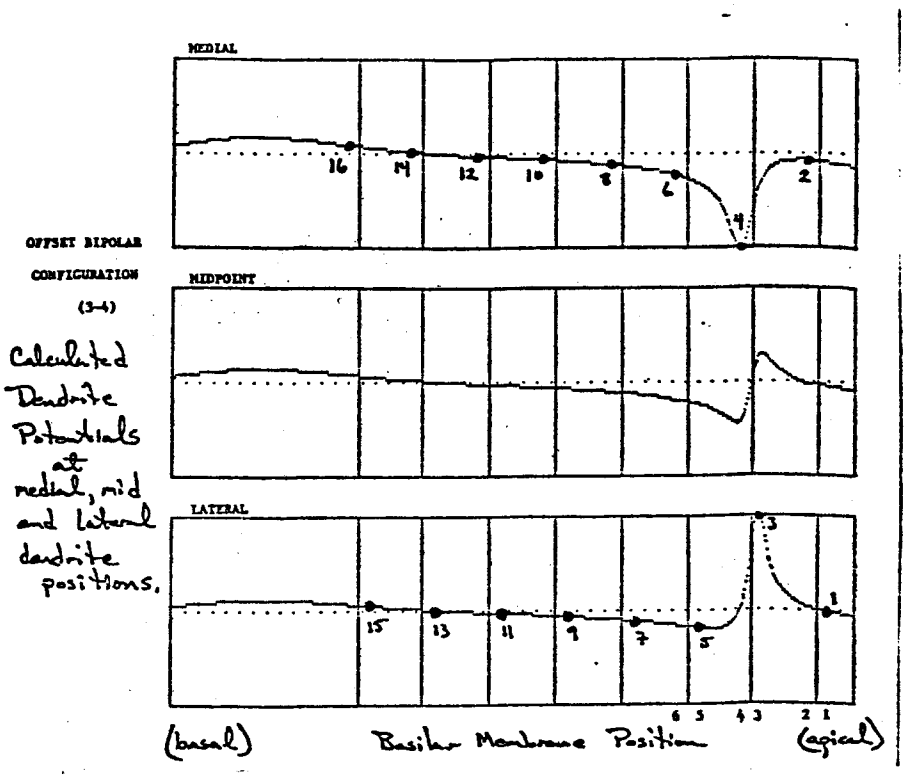

Figure 5.

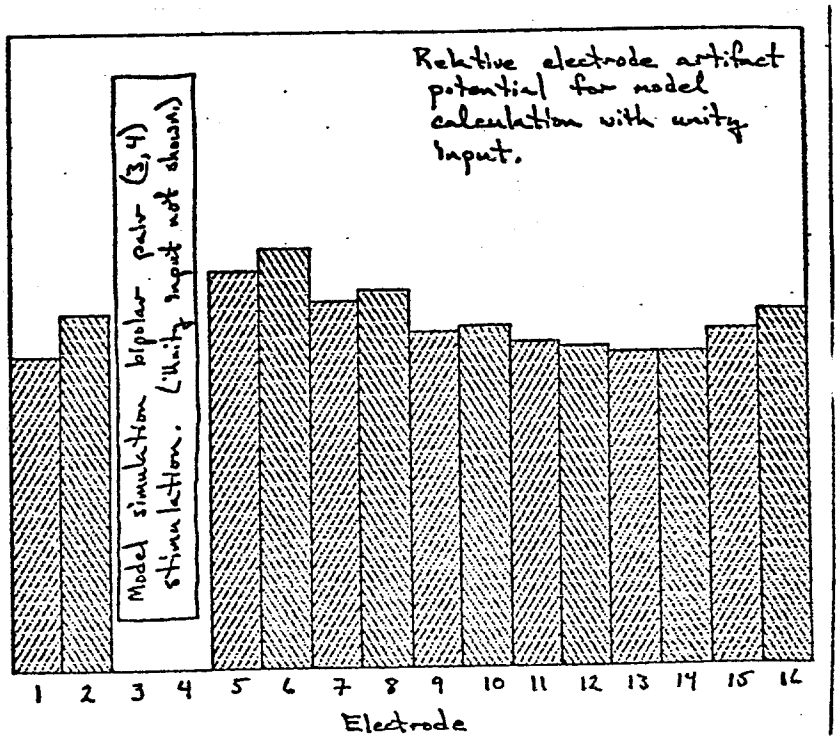

Figure 6.

indicated by its number. The filled circles on the voltage profile curves indicate the approximate voltages that would appear at each of the unstimulated electrodes in the array.

Figure 6 is a histogram plot of the calculated voltages that would appear at each unstimulated electrode, referenced to a remote ground electrode. This plot is essentially a representation of the same electrode potential data from Figure 5. Note that the electrode order along the abcissae in Figure 6 has been reversed from the order in Figure 5. Observe the skewed distribution of voltages around the stimulated pair (electrodes [3] and [4]). Electrodes [1] and [2] show a relatively rapid rate of voltage fall-off as compared to the more gradual voltage decline from electrode [5] to higher number (more basal) electrodes. As would be expected, the gradient is directed away from the stimulated electrode pair. In addition, the more-basal electrode voltages appear to climb slightly at the most-basal positions. It is of interest to compare these model predictions with the measured voltages described below.

Percutaneous Cable Measurements

Figure 7 is a plot of intracochlear potentials measured via a percutaneous cable in patient SG. Bipolar electrode pair [3,4] was stimulated with a subthreshold 26 uA. peak sinusoidal current continuously. Curve STIMULUS is the consequent electrode voltage measured on electrode pair [3,4]. Curve ARTIFACT is the resultant artifact potential measured from electrode [1] with reference to a distant ball electrode placed on the round window. Ordinate scales for each curve are arbitrary. Root-mean-square (RMS) values are calculated for each signal and a final normalized RMS ratio of measured artifact voltage / measured stimulus voltage is obtained. This ratio is referred to as the Relative Transfer Ratio. This measure was repeated for all combinations of bipolar and monopolar electrodes, including both stimulus and artifact measurement configurations. Data were collected at 100, 400, 1000, 4000 and 10000 Hz.

Figure 8 shows the Relative Transfer Ratios measured at electrodes [1] through [16] referenced to the round window for bipolar stimulation of electrode pair [3,4] at 100 Hz. The results show a ratio pattern very similar to that predicted by the mathematical model above (see Figure 6).

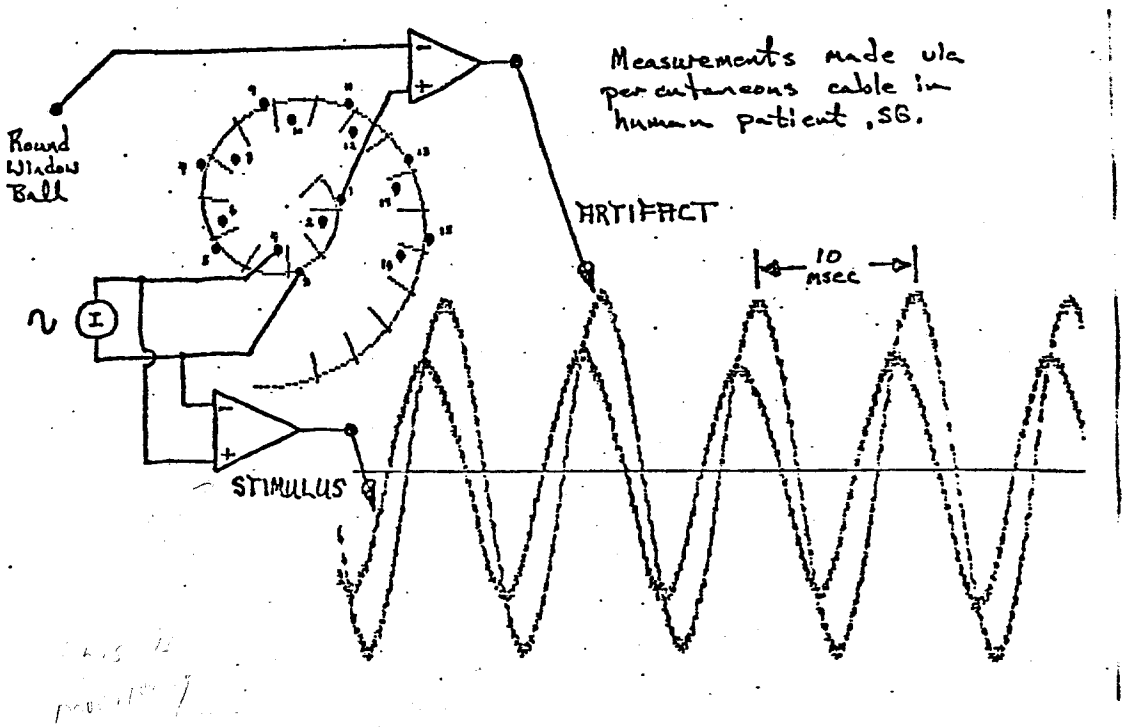
Measurements made via percutaneous cable in human patient, SG.
Round Window Ball
ARTIFACT
10 msec
STIMULUS

Figure 7.

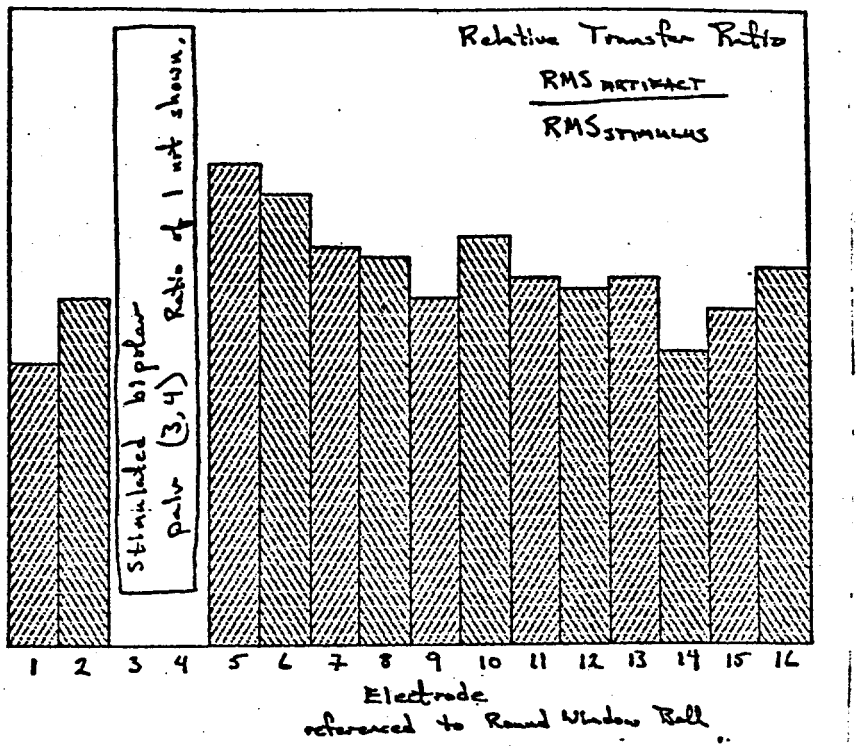

Figure 8.

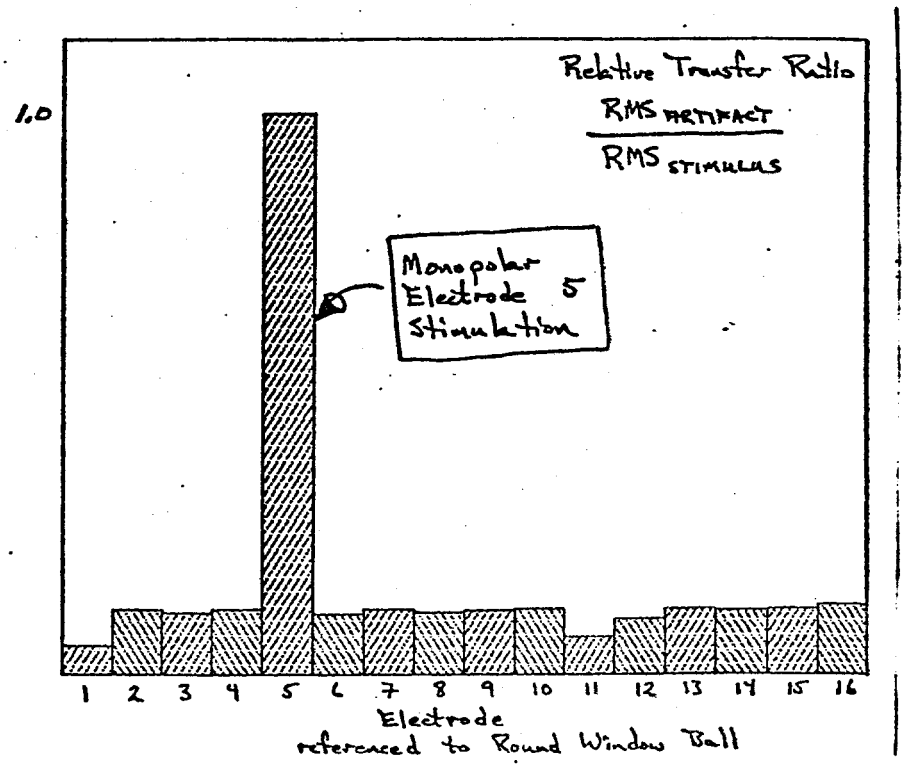

Figure 9.

Figure 9 shows the Relative Transfer Ratios measured at electrodes [1] through [16] referenced to the round window for monopolar stimulation of electrode [5] referenced to a remote ball electrode in the external ear canal. Note that at the non-stimulated electrodes that the Relative Transfer Ratio is essentially the same for each electrode. Exceptions do exist (i.e. electrodes [1], [11], and [12]). This result is consistent with the general notion that the field gradients for monopolar stimulation are small compared to the gradients for bipolar stimulation.

Figures 10 and 11 show the Relative Transfer Ratios measured for artifacts at bipolar pairs with bipolar and monopolar stimulation, respectively. The interpretation of these results is complicated by the fact that these measures reflect the fine structure of the overall field pattern. Further analysis is in progress. These results are included here for purposes of illustration.

Although the results presented here are preliminary, several points are worth considering:

(1) Percutaneous cable measurements of intracochlear fields appear to be possible. Improvements in data quality can be expected with further filtering and cycle-to-cycle averaging of the artifact signals. Further consideration of crosstalk-producing, interlead capacitance within the percutaneous cable is required before analysis and interpretation of higher frequency data can be completed.

(2) Considered alone, the monopolar artifact measurement results for bipolar stimulation with electrode pair [3,4] (Figure 8) appear questionable. However, when compared with the finite-difference model prediction for the same condition (Figure 6) an ordered pattern emerges. This pattern includes a faster artifact potential roll-off across electrodes [1] and [2] as compared to a more gradual artifact decline across electrodes [5] through [11]. This differential in gradients is predicted by the finite-difference model and arises primarily due to the tight, curling geometry of the apical end of the electrode array. The model also predicts a slight increase of artifact potentials across electrodes [12] through [16], due to the basal end of the electrode array curling into the major dipole axis of stimulated bipolar electrode pair [3,4]. Such an increase is not strongly represented in the artifact data but is suggested.

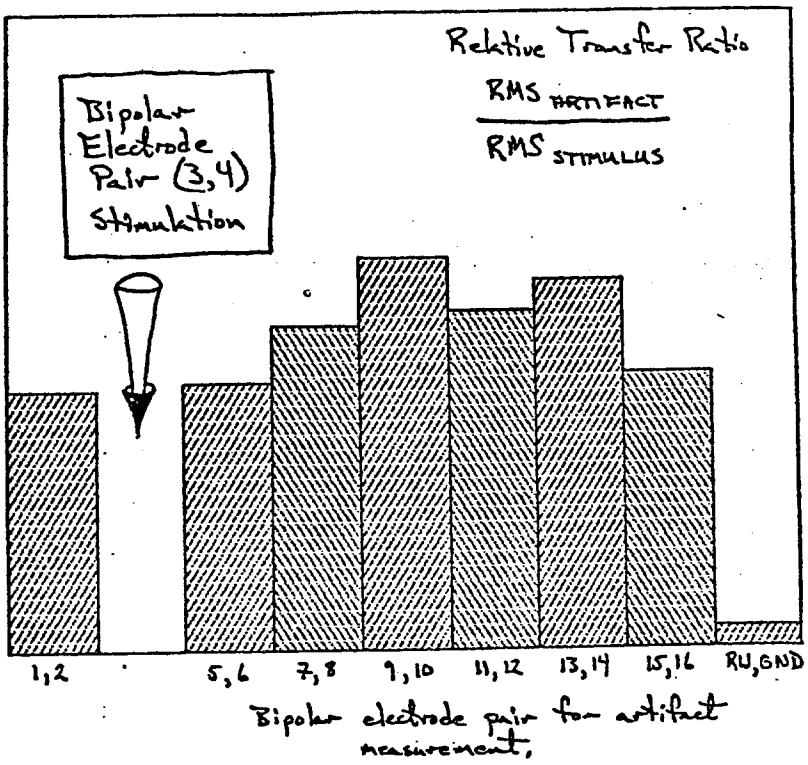

Figure 10.

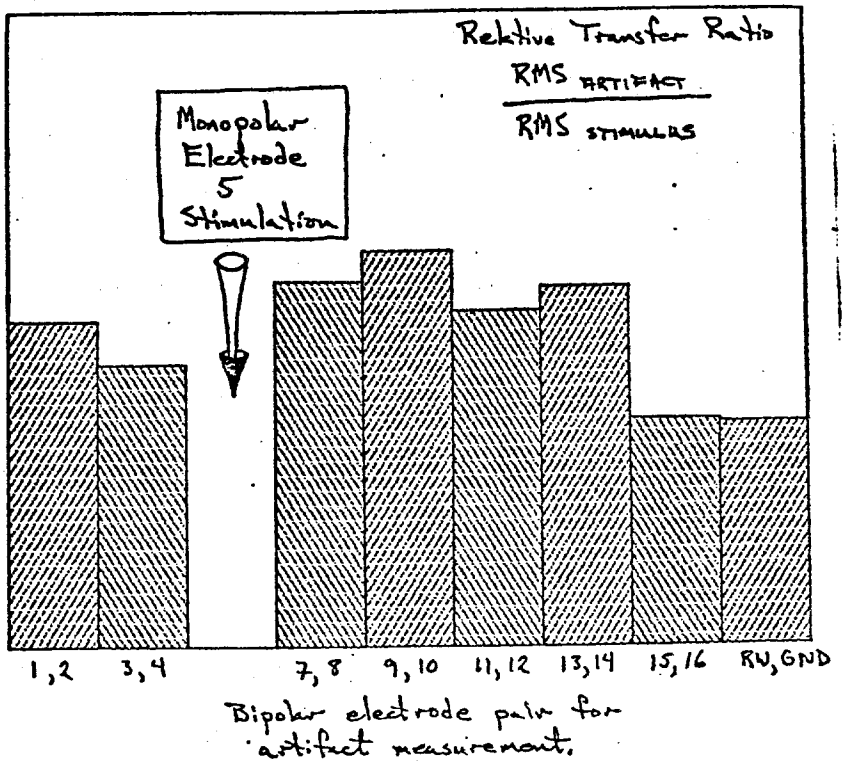

Figure 11.

(3) The monopolar artifact measurement results for monopolar electrode [5] stimulation (Figure 9) indicate an even distribution of artifact components across the array. Exceptions do exist at discrete electrode sites (electrodes [1], [11], [12]). At present the reason for these deviations is not known. Possibly they are due to errors in the recording protocol but may also be due to small local deviations in the field due to patchy survival of dendrites in the local region providing a path for current shunting into the modiolar space. Overall the impression is that monopolar fields are broadly distributed across the cochlea with only small declining gradients.

(4) Interpretation of artifact data recorded from bipolar electrodes (Figures 10 & 11) is clearly more difficult. These data address the fine structure of the stimulus field and will consequently be more sensitive to the distorting effects of local impedance changes within the cochlea (either of tissue boundaries or electrode carrier boundaries). Also, since these bipolar electrodes sample two closely spaced points, the resultant artifact signals are smaller and are therefore more sensitive to contaminating noise and/or percutaneous cable crosstalk. Careful analysis of these particular data is required in conjunction with more highly refined mathematical models of the electrical fields.

(5) Present data indicate that interpretation of spatially distributed samples of field artifacts is greatly enhanced by the availability of model predictions. The facts that the modeled and measured results compare so favorably and that the finite-difference model only really represents electrode geometry (as opposed to the heterogeneous impedance structure of the cochlea) suggest that field patterns within scala tympani cochlea are:

(a) primarily determined by the stimulation electrodes geometry; and

(b) secondarily, determined by the different impedance boundaries and regions of the cochlea.

This observation is not surprising and has been supported by many studies. In more recent years debate seems to have focused upon the relative degree of contribution that the tissue impedance pattern provides. The present

data do not answer this question, but they do suggest that global field patterns in scala tympani are predominately determined by electrode placement and only slightly by tissue impedances, at least in the 100 Hz frequency range. The combined techniques hold promise for exploring the structure of field patterns within the implanted human cochlea.

It is important here to distinguish between field patterns in scala tympani and field patterns along the neural elements. It is entirely possible that tissue impedance plays a considerable role in shaping the potential profiles that exist outside of the neural elements. Good models do not exist presently to describe these mechanisms nor do direct experimental results exist. At this point it is probably safe to speculate that the ensemble pattern of multiple neurons is governed primarily by electrode placement (bipolar vs monopolar) and that the local field outside a single neural element or within a small region is governed primarily by local tissue impedances.

Analysis of these artifact field data from patient SG is proceeding. Once a good feel for these data has been obtained and the method has been refined, the same measures will be obtained from patient MH. Interpretation of data from patient MH will be augmented greatly by the availability of x-rays showing the electrode orientation and spiral shape in two views. (X-rays were taken as a diagnostic medical procedure to manage a sinus infection which occurred during the percutaneous cable testing period.) These measurements will also be extended to include measurement of electrically-evoked neural responses.

IV. Plans for the Next Quarter

The major activity of the next quarter will be continued testing of patient MH. We plan to complete the studies of speech recognition outlined in the Introduction, and to evaluate selected processors with the tests of the Minimal Auditory Capabilities battery (the "MAC" test). In addition, we expect to continue our work on the development of the portable processor described in section II of this report. If all goes well with this last activity, we will also package this processor for at-home use by patient MH. Analysis of field pattern measurements in patient SG will continue in preparation for conducting the same experiment in our current patient MH. Finally, our plans include presentations of project results at the IUPS Satellite Symposium on "Advances in Auditory Neuroscience," to be held in San Francisco this July.

Appendix 1

Summary of Reporting Activity for the Period of March 27 through June 27, 1986, NIH Contract N01-NS-5-2396

The following major presentations were made in the present reporting period:

Wilson, BS: Comparison of strategies for coding speech with multichannel auditory prostheses. Invited faculty lecture presented at the Conference on Speech Recognition with Cochlear Implants, New York University, April 17-19, 1986.

Wilson, BS: Coding strategies for cochlear implants. Invited speaker presentation at the Kresge Hearing Research Institute, University of Michigan, May 22, 1986.

An abstract for the first presentation is shown on the next page of this Appendix.

Comparison of Strategies for Coding Speech with Multichannel Auditory Prostheses

Blake S. Wilson and Charles C. Finley

Neuroscience Program Office
Research Triangle Institute
Research Triangle Park, N.C. 27709

In this presentation we will describe tests we conduct with individual implant patients to evaluate different strategies for coding speech with multichannel auditory prostheses. Results from two patients implanted with the UCSF/Storz electrode array will be presented. Tests with the first patient are completed and tests with the second patient are in progress. The first patient had very poor performance on psychophysical tests and was presumed to have an unfavorable pattern of nerve survival. Moreover, only one of his scores on speech tests (voice/unvoice) was above chance for a "compressed analog outputs" strategy much like the one used in the present UCSF/Storz speech processor and similar to the one used in the Utah/MIT/Symbion device.

With these discouraging results in mind, we evaluated four alternative processing strategies in an attempt to improve this patient's understanding of speech. The basic plan of these other processors was to reduce in steps the temporal and spatial overlap between channels and introduce (in the last two processors) a representation of the linear-prediction residual signal. As we will describe in detail, three of these processors produced percepts that were clearly in the "speech mode," that were spontaneously recognized as the speech tokens delivered to the processor, and that produced test scores well above chance on confusion-matrix material. For this patient changes in the processing strategy produced immediate and compelling differences in recognition performance.

Preliminary results with the second patient indicate that she has a much more favorable pattern of nerve survival than the first patient. Therefore, it will be interesting to see if changes in the processing strategy also have large effects with the second patient and, if so, whether the same strategy or strategies emerge as superior for both patients. Data from the second patient will be available at the time of the conference.